The EMBO Journal (2009) 28, 175–182 | © 2009 European Molecular Biology Organization | All Rights Reserved 0261-4189/09
www.embojournal.org

THE EMBO JOURNAL

Conversion of the 2 Cl^-/1 H^+ antiporter ClC-5 in a NO_3^-/H^+ antiporter by a single point mutation

Giovanni Zifarelli and Michael Pusch*

Istituto di Biofisica, CNR, Via De Marini, Genova, Italy

Several members of the CLC family are secondary active anion/proton exchangers, and not passive chloride channels. Among the exchangers, the endosomal ClC-5 protein that is mutated in Dent's disease shows an extreme outward rectification that precludes a precise determination of its transport stoichiometry from measurements of the reversal potential. We developed a novel imaging method to determine the absolute proton flux in *Xenopus* oocytes from the extracellular proton gradient. We determined a transport stoichiometry of 2 Cl^-/1 H^+. Nitrate uncoupled proton transport but mutating the highly conserved serine 168 to proline, as found in the plant NO_3^-/H^+ antiporter atClCa, led to coupled NO_3^-/H^+ exchange. Among several amino acids tested at position 168, S168P was unique in mediating highly coupled NO_3^-/H^+ exchange. We further found that ClC-5 is strongly stimulated by intracellular protons in an allosteric manner with an apparent pK of ~7.2. A 2:1 stoichiometry appears to be a general property of CLC anion/proton exchangers. Serine 168 has an important function in determining anionic specificity of the exchange mechanism.

The EMBO Journal (2009) **28,** 175–182. doi:10.1038/emboj.2008.284; Published online 8 January 2009
Subject Categories: membranes & transport
Keywords: anion; antiporter; chloride; ion channel; proton transport

Introduction

The CLC protein family is of paramount physiological importance as underscored by the presence of its members in all phylae (Maduke *et al*, 2000) and their involvement in human genetic diseases (Zifarelli and Pusch, 2007; Jentsch, 2008). As the first members to be identified and to be extensively studied were Cl^- channels, it was thought that this would be a common feature of all CLC proteins. This was the case also for ClC-5 when its first electrophysiological characterization was reported (Steinmeyer *et al*, 1995). However, more recent studies triggered by the finding that the bacterial ClC-ec1 is actually a Cl^-/H^+ antiporter (Accardi and Miller, 2004) led to the conclusion that similar to ClC-ec1, also ClC-4 and ClC-5 are Cl^-/H^+ antiporters in which the movement of Cl^- is thermodynamically coupled to the transport of protons in the opposite direction (Picollo and Pusch, 2005; Scheel *et al*, 2005).

Despite this functional diversity, the overall protein architecture is conserved across the whole family. CLCs are composed of two subunits, each harbouring an ion translocation pathway (Ludewig *et al*, 1996; Middleton *et al*, 1996; Weinreich and Jentsch, 2001; Dutzler *et al*, 2002).

ClC-5 is part of a family branch comprising also ClC-3 and ClC-4 (Steinmeyer *et al*, 1995). It is mostly expressed in the proximal tubule, a segment of the nephron responsible for the reuptake of small molecular weight proteins (Günther *et al*, 1998). It is mutated in Dent's disease, a disorder characterized by defective endocytosis leading to kidney stones and renal failure (Lloyd *et al*, 1996). It has been proven that ClC-5 colocalizes with an endosomal H^+-ATPase and with endosomal markers and endocytosed proteins, suggesting a function in the acidification of early endosomes (Günther *et al*, 1998, 2003; Piwon *et al*, 2000) (for review, refer Jentsch, 2005; Zifarelli and Pusch, 2007). In support of this view, ClC-5 knockout mice showed an impaired endocytosis (Piwon *et al*, 2000) and a reduced ability to accumulate H^+ and Cl^- in the endosomes (Piwon *et al*, 2000; Hara-Chikuma *et al*, 2005).

In spite of the considerable insights into the function of ClC-5, our knowledge of its molecular function and biophysical properties remains very limited. We have recently proposed a model in which transport activity in ClC-5 occurs in bursts. Within each burst, transport is very fast, in the order of 10^5 ions/s (Zdebik *et al*, 2008). According to this model, the unitary transport properties of ClC-5 can be estimated using non-stationary noise analysis, a method that is classically applied to ion channels but not transporters. The apparent single transporter conductance (~0.5 pS; Zdebik *et al*, 2008) reflects the mean transporter current once it is in the active state (Hilgemann, 1996).

However, several aspects of the ClC-5 function remain to be investigated; one of the most prominent is the transport stoichiometry of the exchanger, that is, the number of Cl^- ions transported per each proton. The bacterial ClC-ec1, for which a simple estimate of the transport stoichiometry can be obtained from reversal potential measurements (Accardi and Miller, 2004), shows a 2 Cl^-/1 H^+ stoichiometry with almost no slippage (Accardi and Miller, 2004; Accardi *et al*, 2006; Nguitragool and Miller, 2006; Walden *et al*, 2007). Unfortunately, this approach is not feasible for ClC-5 because currents mediated by the transporter are extremely outwardly rectifying (Steinmeyer *et al*, 1995; Friedrich *et al*, 1999). Initial rough estimates for the Cl^-/H^+ stoichiometry ranged from 1 to 5 (Picollo and Pusch, 2005; Scheel *et al*, 2005). These measurements were, however, associated with a large error. We have now developed a new imaging method to determine the absolute proton flux in *Xenopus* oocytes from the extracellular proton gradient, and determined a 2:1 Cl^-/H^+ stoichiometry, similar to the bacterial ClC-ec1. A 2:1 stoichiometry was also described for the plant vacuolar atClCa NO_3^-/H^+ transporter (De Angeli *et al*, 2006). From a

*Corresponding author. Istituto di Biofisica, CNR, Via De Marini, 6, I-16149 Genoa, Italy. Tel.: +39 0106475 561/522; Fax: +39 0106475 500; E-mail: pusch@ge.ibf.cnr.it

Received: 30 June 2008; accepted: 8 December 2008; published online: 8 January 2009

mechanistic viewpoint, the different anion specificity is particularly interesting because NO_3^- and other polyatomic anions lead to a partial uncoupling of H^+ transport in ClC-ec1 and ClC-5 (Nguitragool and Miller, 2006; Zdebik *et al*, 2008). However, the molecular mechanism underlying the different anion specificity of ClC-ec1 and ClC-5 compared with the plant atClCa is unknown.

Here, we found that the serine residue S168 of ClC-5 is critical for anion selectivity and coupling efficiency. Mutating this residue into a proline is sufficient to convert ClC-5 into a NO_3^-/H^+ antiporter. This serine in conserved in most Cl^- channels and transporters; in ClC-ec1, it is involved in the coordination of Cl^- ions (Dutzler *et al*, 2002, 2003), and in ClC-0 it has been shown to have a critical function for ion selectivity, single-channel conductance, and gating.

In addition, in this study, we directly investigate for the first time the regulation of ClC-5 by intracellular pH. Intracellular pH changes in response to a variety of stimuli and influences a number of cellular functions (Roos and Boron, 1981). Furthermore, there is increasing evidence that such pH changes are not uniform but, instead, subcellular domains might experience specific pH shifts (Pastoriza-Munoz *et al*, 1987; Aw and Jones, 1989; Swietach *et al*, 2005).

Results

Validation of the fluorescence-based proton flux assay using a sucrose/proton co-transporter

We developed an imaging system to quantify the proton flux across the plasma membrane of *Xenopus* oocytes. The setup is schematically shown in Figure 1A. Changes in the extracellular proton concentration close to the oocyte surface were imaged using the pH-sensitive dye BCECF. Each measurement was accompanied by a calibration of the BCECF solution (without oocyte) before and after the experiments. An example of calibration is shown in Figure 1B. It can be seen that the ratio change of the BCECF fluorescence is linearly related to the total amount of protons added (see the straight line in Figure 1B). This linearity is very convenient because it allows working on differential signals (e.g., 'baseline' subtraction). The analysis of the extracellular BCECF fluorescence is described in detail in the Supplementary data section.

To validate the method, we applied it on the maize sucrose/proton co-transporter ZmSut1 (Carpaneto *et al*, 2005). The only charged substrate carried by this transporter are protons such that, ideally, the electrically recorded sucrose-induced transport current should coincide with the proton current determined by the fluorescent assay. A typical experiment is illustrated in Figure 1C. The proton gradient ΔH_{tot} is plotted as a function of the radius for various time points (see legend for symbols) together with the theoretical fit (lines). In this particular experiment, the proton current from the fluorescence data was estimated as 159 nA, whereas for the electrical current, we measured a value of 160 nA, being thus in excellent agreement. Figure 1D shows average values of the ratio of the electrical current and the proton-current measured at various voltages. The agreement between these two independent estimates supports the validity of the fluorescence-based assay of proton flux.

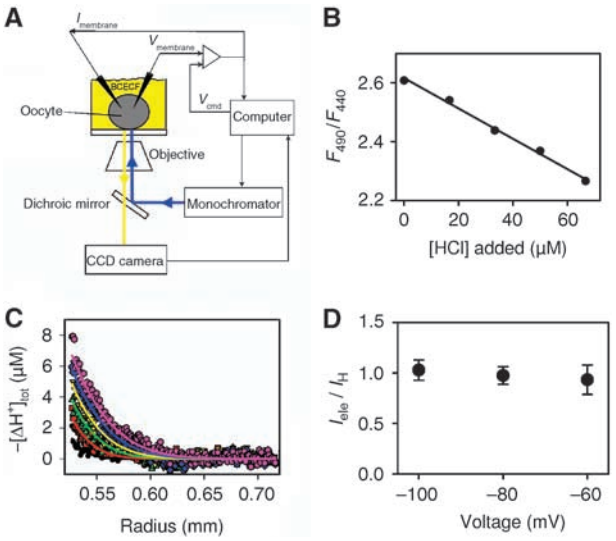

Figure 1 Fluorescence assay for the measurement of proton fluxes. (**A**) Schematic representation of the experimental setup. (**B**) Representative calibration curve obtained measuring the ratio of the BCECF fluorescence emission excited at 490 and 440 nm wavelength as a function of the amount of HCl added. The straight line has a slope of −193 μM/ratio unit. (**C**) $\Delta[H^+]_{tot}$ change evoked by sucrose application in an oocyte expressing ZmSut1 at −80 mV plotted as a function of the distance from the oocyte centre at different time points (black circles, 0.3 s; red squares, 0.6 s; green triangles, 0.9 s; yellow triangles, 1.2 s; blue diamonds, 1.5 s; pink hexagons, 1.8 s; data show the negative $\Delta[H^+]_{tot}$ (i.e., the transporter induces alkalinization). The fit with the theoretical prediction (Equation (C), Supplementary data) resulted in an estimated proton current of 159 nA and a diffusion coefficient of 5×10^{-10} m^2/s (solid lines). The electrical current was 160 nA in this experiment. (**D**) Average values for the ratio of the sucrose induced electrical current, I_{ele}, and the proton current, I_H, estimated from the fluorescence assay at different membrane voltages (error bars indicate s.e.m., $n \geqslant 6$).

Transport stoichiometry of ClC-5

Next, we applied the same method to ClC-5. Results for a typical experiment (at 80 mV) are shown in Figure 2A. In this case, the proton current, I_H, was estimated at 0.56 μA, whereas the electrical current, I_{ele}, was measured at 1.51 μA. Assuming a stoichiometric coupling of N chloride ions for each transported proton, the electrical current, being the sum of the proton current and the chloride current, is given by

$$I_{ele} = I_{Cl} + I_H = (N+1)I_H$$

and thus

$$N = \frac{I_{ele} - I_H}{I_H}.$$

This ratio is plotted in Figure 2B as a function of the membrane voltage. It can be seen that the stoichiometric coupling ratio is close to 2 and it is independent of the applied voltage. The overall average including all voltages is 1.95 ± 0.11 (s.e.m., $n = 29$).

Previous qualitative experiments have shown that H^+ coupling to anion transported is significantly weakened if NO_3^- or SCN^- are substituted for Cl^- (Zdebik *et al*, 2008). In fact, applying our fluorescence-based H^+ transport assay, we determined an approximately six- to ten-fold reduction of the stoichiometric coupling ratio for NO_3^-/H^+ antiport (Figure 2C). Under such conditions of weak coupling and

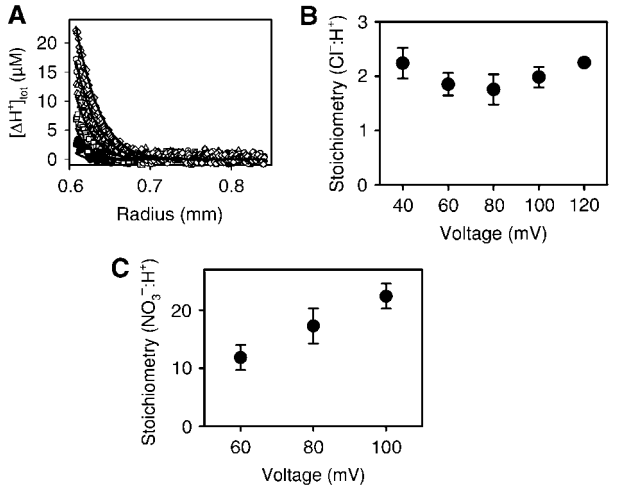

Figure 2 Transport stoichiometry of ClC-5. (**A**) Typical experiment showing acidification induced by a test pulse to 80 mV as a function of the distance from the oocyte centre at different time points (filled circles, 0.8 s; squares, 1.6 s; triangles, 2.4 s; open circles, 3.2 s; diamonds, 4 s; note that the data were taken at a certain distance from the oocyte surface to avoid buffer saturation (Zifarelli *et al*, 2008); the oocyte radius was 0.57 mm in this case). The fit with the theoretical prediction (Equation (C), Supplementary data) resulted in an estimated proton current of 0.56 μA and a diffusion coefficient of 4.5×10^{-10} m^2/s (solid lines). The electrical current was measured at 1.51 μA in this experiment. (**B**) Average of the apparent Cl^-/H^+ stoichiometry ratios obtained at various voltages (error bars indicate s.e.m.; $n \geqslant 5$, except 120 mV for which $n = 3$). (**C**) Average of the apparent NO_3^-/H^+ stoichiometry ratios obtained at various voltages (error bars indicate s.e.m.; $n \geqslant 3$).

large turnover, the classical distinction between a coupled transporter and a passive channel becomes fuzzy, highlighting the positioning of CLC proteins at an ambiguous interface between these two classes of membrane proteins (Gadsby, 2004; Miller, 2006).

Conversion of ClC-5 into a NO_3^-/H^+ exchanger

NO_3^- uncouples H^+ transport in ClC-5 and ClC-ec1 (Nguitragool and Miller, 2006; Zdebik *et al*, 2008), whereas the plant atClCa shows coupled NO_3^-/H^+ antiport (De Angeli *et al*, 2006). Inspecting the sequence of these three transporters in the highly conserved ion-binding regions reveals that atClCa carries a proline at position 168 (numbering of ClC-5), whereas ClC-ec1, ClC-5, as well as all other known CLC Cl^- channels and Cl^-/H^+ antiporters have a serine at the equivalent position (Figure 3A).

Therefore, we introduced the mutation S168P in ClC-5 and investigated its properties. Currents mediated by this mutant in the standard Cl^- solution were outwardly rectifying as WT, but their magnitude was barely above background (Figure 3C). Exchanging extracellular Cl^- with NO_3^- led to a dramatic increase of outward currents (corresponding to inward anion flow) (Figure 3C), suggesting a significant change of anion selectivity (compare with WT traces, Figure 3B). In addition, for the mutant, the activation kinetics of the currents were significantly slower and more pronounced (compare Figure 3B and C).

Comparing the currents in the positive voltage range in the presence of various extracellular anions, we established that S168P has a conductivity sequence ($NO_3^- > I^- > Br^- \sim Cl^-$) (Figure 3D), which differs from that of WT ClC-5

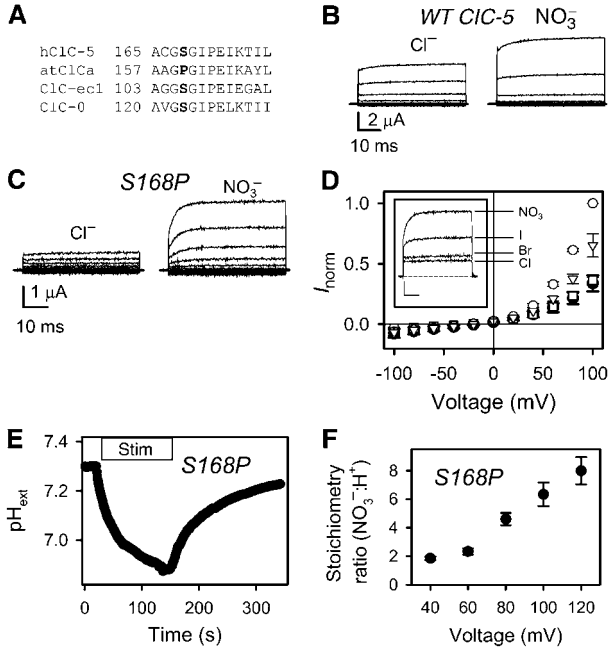

Figure 3 Analysis of the S168P mutant. (**A**) The alignment of a sequence stretch comprising the conserved serine (shown in bold) for hClC-5, the *Arabidopsis thaliana* NO_3^-/H^+ antiporter atClCa, the Cl^-/H^+ antiporter from *Escherichia coli* ClC-ec1 and the Cl^- channel ClC-0. (**B**, **C**) representative currents from WT ClC-5 (B) and the mutant S168P (C) in extracellular solutions containing Cl^- (left) or NO_3^- (right). Voltages range from +100 to −80 mV in 20 mV steps. (**D**) Current–voltage relationship for S168P in extracellular solutions containing Cl^- (filled circles) ($n = 9$), NO_3^- (open circles) ($n = 10$), Br^- (squares) ($n = 3$), I^- (triangles) ($n = 3$). Inset shows current traces from one oocyte at 100 mV in the presence of the same anions. Scale bars indicate 0.5 μA and 10 ms, respectively. (**E**) Representative measurement of the extracellular acidification using a pH-sensitive microelectrode placed close to the oocyte surface produced by the activation of S168P in extracellualr NO3 with repetitive voltage pulses to 100 mV. The stimulation period is indicated by the bar. (**F**) Voltage dependence of the apparent NO_3^-/H^+ transport stoichiometry of S168P determined as in Figure 2. Error bars indicate s.e.m. ($n \geqslant 6$).

Table I Conductivity sequences among halide ions and nitrate for WT ClC-5 and various mutants of residue 168

Residue	Conductivity sequence
S (WT)	$NO_3 > Cl > Br > I$
A	$NO_3 > Br \sim I \sim Cl$
G	$NO_3 > Cl > Br > I$
P	$NO_3 > I > Br > Cl$
T	$NO_3 > I > Br > Cl$

($NO_3^- > Cl^- > Br^- > I^-$) (Steinmeyer *et al*, 1995) (see Table I) but is very similar to that of atClCa ($NO_3^- \sim I^- > Br^- > Cl^-$) (De Angeli *et al*, 2006).

We next investigated whether NO_3^- transport by this mutant is coupled to H^+ movement using an extracellular pH-sensitive microelectrode (Picollo and Pusch, 2005). Figure 3E shows that NO_3^- transport, activated by positive potentials, produces a significant acidification of the extracellular solution, which readily reverses upon switching off of the clamp, suggesting a stronger coupling of NO_3^- to H^+ transport in the mutant compared with WT (Zdebik *et al*, 2008). Furthermore,

measurements performed with an inwardly directed pH gradient show that the outward movement of protons is produced by an active transport mechanism, proving a thermodynamic coupling between NO_3^- and H^+ movement through S168P (Supplementary Figure 2).

We quantitatively investigated the NO_3^-/H^+ transport stoichiometry of S168P using our fluorescence assay. We found that, at moderately positive voltages (40 and 60 mV), the NO_3^-/H^+ stoichiometry was close to 2, whereas H^+ transport became less coupled to anion transport at more positive voltages (Figure 3F), but still much strongly coupled than WT NO_3^-/H^+ exchange (Figure 2C).

Analysis of transport activity of other mutants at position 168

To systematically study the effect of amino-acid substitutions at position 168 on transport properties, we additionally mutated S168 into A, C, G, H, L, N, Q, T, and Y. Among these mutants, only S168A, S168G, and S168T yielded currents above background in Cl^-, Br^-, I^-, or NO_3^- containing solutions. All mutants showed a reduced current expression compared with WT (data not shown). Preliminary results indicated that all mutants (including S168P) exhibited coupled Cl^-/H^+ exchange with a stoichiometry of roughly 2:1 at voltages $\leqslant$80 mV (G. Zifarelli and M. Pusch, unpublished data). S168A and S168T, but not S168G, changed the conductivity sequence compared with WT as documented in Table I and Supplementary Figure 3. In further experiments, we concentrated on the ability of the mutants to select for NO_3^- compared with Cl^- in coupled transport. We first performed a detailed analysis of the relative current magnitude in NO_3^- compared with Cl^- for the various mutants (Figure 4A). As for WT, all mutants show a preference for NO_3^- transport compared with Cl^- transport. However, for the two mutants S168T and S168P, this preference is much more pronounced. S168A shows an intermediate phenotype, whereas for S168G, Cl^- currents are only slightly smaller than NO_3^- currents, thus being similar to WT (Figure 4A). But is NO_3^- transport coupled to H^+ transport as in S168P or uncoupled as in WT? To address this question, we determined the relative coupling efficiency, e_{rel}, as described in Materials and methods, comparing the acidification measured with a pH-sensitive microelectrode in Cl^- and NO_3^- on the same oocytes (see Supplementary Figure 4 for representative recordings). A value of $e_{rel}=1$ means that NO_3^- transport and Cl^- transport are equally well coupled to H^+ counter-transport. A small value of e_{rel} indicates inefficient NO_3^-/H^+ exchange (see Equation (2)). Figure 4B shows the values of e_{rel} for WT and the four functional S168 mutants at 60, 80, and 100 mV. In agreement with the fluorescence data, WT exhibits inefficient and voltage-dependent NO_3^-/H^+ transport coupling. S168P is the only mutant that shows a similar coupling efficiency of NO_3^-/H^+ exchange and Cl^-/H^+ exchange. S168A, S168G, and S168T show an intermediate phenotype, with NO_3^- transport being less coupled than Cl^- transport. Thus, among all mutants tested, S168P is unique in that it strongly selects for NO_3^- against Cl^-, maintaining stoichiometrically coupled H^+ antiport.

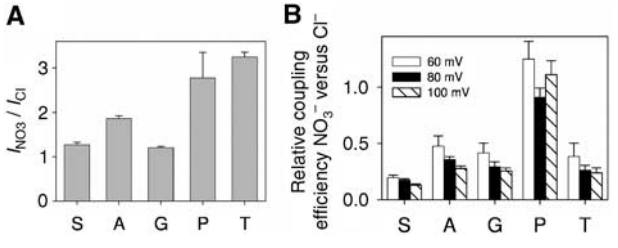

Figure 4 Nitrate over chloride preference of WT and mutants at position 168. (**A**) Ratio between current values measured at 80 mV in extracellular solutions containing NO_3^- and Cl^-, respectively, for WT and the indicated mutants of S168. Currents were leak-subtracted. Error bars indicate s.e.m. ($n\geqslant15$). (**B**) For each potential (symbols are indicated in the figure), we calculated the relative coupling efficiency, e_{rel} (as described in Materials and methods), comparing acidification (measured with a pH-sensitive microelectrode) and currents in Cl^- and NO_3^- containing extracellular solutions. Error bars indicate s.e.m. ($n\geqslant5$).

Intracellular pH dependence of ClC-5

To gain more insight in the regulation of ClC-5 by pH, we studied its dependence on the intracellular H^+ concentration using inside-out patch clamp recordings. Current traces for a typical experiment are shown in Figure 5A. Compared with the physiological pH 7.3, ClC-5 currents are dramatically

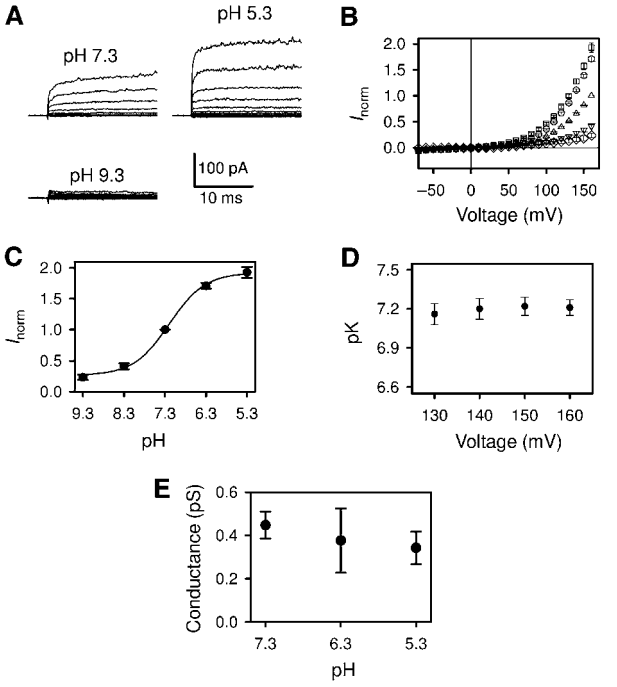

Figure 5 Dependence of ClC-5 on the intracellular proton concentration. (**A**) Representative recordings from one inside-out patch perfused with intracellular solutions at different pH values as indicated. Voltages range from +160 to −60 mV in 20 mV steps. (**B**) Normalized current–voltage relationships at pH 5.3 (squares) ($n=9$), 6.3 (circles) ($n=8$), 7.3 (triangles up) ($n=18$), 8.3 (triangles down) ($n=5$), 9.3 (diamonds) ($n=3$). Currents were normalized to the current measured at pH 7.3 at 160 mV. (**C**) Plot of normalized currents at 160 mV as a function of pH. The solid line is a Hill fit as described in the main text with $I_{max}=1.9$, $I_{min}=0.3$, $K=6.2\times10^{-8}$ M (pK = 7.21). (**D**) Plot of the mean values of the pK obtained as in C, versus voltage. (**E**) Average values of the apparent single channel conductance measured by noise analysis performed on patches perfused with solutions at pH 7.3 ($n=8$), pH 6.3 ($n=5$), pH 5.3 ($n=4$). Error bars indicate s.e.m.

activated by acidic pH, and almost completely suppressed at alkaline pH (Figure 5A and B). We quantified the pH dependence at the most positive voltages (which allowed a reliable determination of the current amplitudes). An example of the analysis performed at 160 mV is shown in Figure 5C. The activation can be well described by a simple 1:1 binding curve of the form

$$I_{norm} = I_{min} + (I_{max} - I_{min})\frac{H/K}{1 + H/K}$$

where H is the free proton concentration, K the apparent binding constant ($pK = -\log(K)$), I_{min} and I_{max} are the minimal and the maximal values, respectively. The apparent pK is ~7.2, very close to the physiological intracellular pH and is voltage independent (in the range 130–160 mV) (Figure 5D).

The increase of currents at acidic pH could simply reflect a larger turnover of the transporter, enabled by the larger H^+ concentration. Alternatively, protons could regulate the probability of the transporter to be in an active state.

To discern between these possibilities, we applied nonstationary noise analysis. This method is classically applied to ion channels but not to transporters. However, we have shown previously that the spectral noise properties of ClC-5 are consistent with the idea that the transporter is 'gated', that is, fluctuates between active and inactive states (Zdebik *et al*, 2008). Because, as for ion channels, individual transport events are not resolved, the noise is dominated by the gating noise (Hilgemann, 1996). Thus, non-stationary noise analysis can be used to obtain estimates of the transporter turnover during the bursts of activity. We will call this quantity the 'single transporter current'.

For pH $\leqslant$7.3, we found that the single transporter current was independent of pH (Figure 5E). This result suggests that the current increase is not caused by an increased turnover, but reflects an increased probability of the gated transporter to be in an active state. Unfortunately, for pH>7.3, currents were too small to allow a reliable estimate of the single transporter current. Thus, we cannot exclude that the reduction of currents at alkaline pH is caused, at least partially, by a reduced turnover.

To further test the hypothesis that the current increase at acidic pH reflects a regulation of the probability of ClC-5 to be in an active state, we exploited the fact that substitution of extracellular Cl^- with NO_3^- leads to a large uncoupling of anion and proton transport, H^+ transport thus being of relatively minor importance for the overall transport activity. Thus, at difference with the situation in the presence of Cl^-, in NO_3^- a smaller pH effect may be expected if pH directly affects the turnover. On the other hand, a similar pH effect is expected in NO_3^-, if protons modulate the probability of the transporter to be in an active state. Furthermore, ClC-5 shows a more pronounced activation time-course in NO_3^-, rendering non-stationary noise analysis more reliable. As shown in Figure 6A, pH strongly affects ClC-5 currents when NO_3^- is the transported anion. In particular, the pH regulation (Figure 6B) is very similar in comparison with the measurements in the presence of Cl^- (see Figure 5C). Furthermore, the single transporter current is independent from pH_{int} in the range 5.8 to 7.3 (Figure 6C). These measurements confirm the conclusion that pH_{int} mostly regulates the probability of the transporter to be in an active state with little influence on the turnover rate.

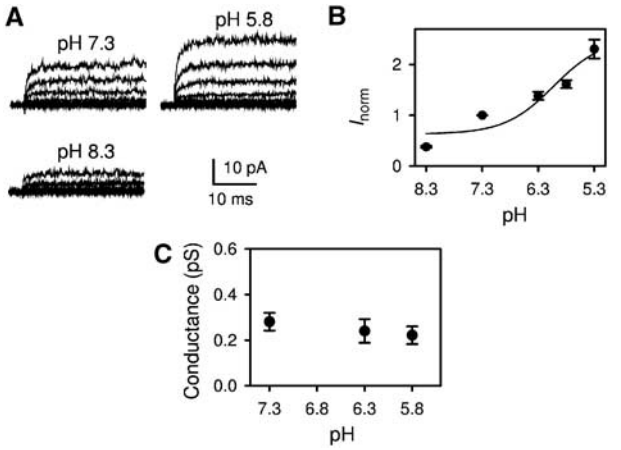

Figure 6 Internal pH dependence of ClC-5 in the presence of external NO_3^- (**A**) representative recordings from one inside-out patch perfused with intracellular solutions at different pH values as indicated. Voltages range from +160 to −60 mV in 20 mV steps. (**B**) Plot of normalized currents at 140 mV as a function of pH. The solid line is a Hill fit as described in the main text with $I_{max} = 2.5$, $I_{min} = 0.63$, $K = 9.4 \times 10^{-7}$ M (pK = 6.03). (**C**) Average values of the apparent single-channel conductance with external NO_3^-. Error bars indicate s.e.m.

Discussion

There is solid evidence that the major physiological function of ClC-5 is related to the acidification of endosomes, consistent with its localization in segments of the nephron with a high endocytic activity and with its involvement in Dent's disease, caused by a defective endocytosis. It was assumed previously that ClC-5 was a Cl^- channel, and this would naturally propose its molecular function: to provide a Cl^- conductance serving as an electrical shunt to allow efficient endosomal accumulation of protons by the V-type ATPase. The finding that ClC-5 is not a Cl^- channel but a Cl^-/H^+ antiporter (Picollo and Pusch, 2005; Scheel *et al*, 2005) called for a thorough revaluation of this picture. However, a better understanding of the physiological function of ClC-5 is inextricably intertwined with a broader knowledge of its basic, biophysical properties. Among the biophysical features with direct physiological implications, in this work, we focused our attention on three problems. The first, and most important one, is the stoichiometry of transport, which determines the degree of coupling between Cl^- and H^+. Secondly, we identified a residue that determines the anion selectivity and coupling efficiency of the transporter. Lastly, we investigated the dependence of the transport activity on the cytoplasmic proton concentration. To tackle these questions, we used different approaches.

To study the stoichiometry of transport in ClC-5, we developed a new imaging method that allowed direct quantification of the outward proton flux. Taking advantage of this method, we found a voltage-independent stoichiometry of 2 Cl^-/1 H^+. The same stoichiometry has been found for the bacterial ClC-ec1 (Accardi and Miller, 2004), for the plant atClCa (De Angeli *et al*, 2006), and for the lysosomal ClC-7 (Graves *et al*, 2008). Thus, a 2:1 stoichiometry seems to represent a general feature of the Cl^-/H^+ antiport activity in the CLC family, possibly implying a similar coupling mechanism. This tight coupling suggests that the main

physiological function of ClC-5 is not only to provide a Cl^- shunt conductance to assist the efficient accumulation of H^+ by the V-type ATPase, but also to actively contribute to the endosomal acidification loading directly protons into the endosomes using the Cl^- gradient. Alternatively, it is conceivable that the tight coupling between Cl^- and H^+ movement can provide a means to regulate endosomal chloride concentration (Zifarelli and Pusch, 2007; Jentsch, 2008). Further studies are, however, required to clarify this point.

Polyatomic anions, like NO_3^-, are transported by ClC-5 and the bacterial ClC-ec1 with much weaker coupling to the H^+ movement in comparison with Cl^- (Nguitragool and Miller, 2006; Zdebik *et al*, 2008), probably because these anions induce slippage (Nguitragool and Miller, 2006), whereas NO_3^- is transported by the plant atClCa with a coupled 2 NO_3^-/1 H^+ stoichiometry (De Angeli *et al*, 2006). An understanding of the molecular determinants responsible for such a different anion selectivity is of relevance in both biophysical and physiological terms. We have found here that serine 168 is critical for the anion selectivity. This residue is conserved in most Cl^- channels and Cl^-/H^+ antiporters of the CLC family. Its mutation to proline, as found in the plant NO_3^-/H^+ antiporter atClCa, alters the conductivity sequence compared with WT (Steinmeyer *et al*, 1995) and makes it similar to what is found for atClCa (De Angeli *et al*, 2006). This finding, by itself, may not seem surprising, as NO_3^- permeates also the WT. However, there is an important difference: in WT ClC-5, NO_3^- permeation is almost uncoupled from H^+ transport, whereas for S168P, NO_3^- transport is much tightly coupled to H^+ movement.

An important function of the serine in the 'signature sequence' GSGIPE for CLC channel gating and selectivity has been established more than a decade ago (Ludewig *et al*, 1996). Its function became evident when Dutzler *et al* (2002, 2003) identified S107 (corresponding to S168 in ClC-5) as one of the residues that coordinates Cl^- ions in the crystal structure of ClC-ec1. In ClC-5, the corresponding S168 most likely has the same critical function. To achieve a deeper insight into the mechanism of anion selectivity, we mutated S168 to several other residues. Among all mutations, S168P is unique in that it greatly diminishes transport of Cl^- and at the same time confers highly coupled NO_3^-/H^+ antiport activity to ClC-5, the same features observed in the activity of the plant atClC-a (De Angeli *et al*, 2006) and that are critical for plant anion homoeostasis. This result shows that S168 is the major determinant of anion selectivity. Interestingly, a proline at the position corresponding to 168 is found only in plant CLCs. Three of the seven *Arabidopsis* CLCs contain a serine and four carry a proline. On the basis of our results, the latter ones are all predicted to be NO_3^-/H^+ exchangers, for which the exclusion of Cl^- as a transported anion is physiologically important. A BLAST search revealed that in eukaryotic CLCs, apart from serine and proline, only alanine and glycine are found at the position corresponding to 168, and only in unicellular organisms. These observations are in agreement with our mutational analysis. Most mutations introduced at position 168 resulted in a non-functional transporter, highlighting the strict constraints that the residue at position 168 must obey to preserve transport (and/or correct membrane targeting). Apart from serine and proline, only the residues alanine, glycine, and threonine were tolerated at position 168. We are in no position to propose a stringent structural interpretation of the mutants' behaviour, but, due to the peculiar chemical properties of proline, its introduction can be expected to lead to a backbone rearrangement. The fact that S168P is the only mutant that dramatically changes transport properties is compatible with the hypothesis that such a structural change underlies the specific features of S168P, and this would also explain the relatively minor effect of the other mutants. Clearly, structural studies are required to clarify this point.

Surprisingly, mutant S168G is very similar to WT with efficient H^+ pumping and identical ion selectivity. The structure of a construct of the bacterial ClC-ec1 harbouring the S107G mutation (corresponding to S168G of ClC-5) showed no major alterations of secondary structure (Lobet and Dutzler, 2006). However, the S107G mutation in ClC-ec1 is almost completely uncoupled (Jayaram *et al*, 2008), suggesting significant differences between ClC-5 and ClC-ec1 in the detailed mechanism of anion binding.

Intracellular pH is a fundamental physiological parameter that both reflects and influences many cellular functions, but its effect on ClC-5 has not been investigated yet. Here, we found that intracellular protons activate ClC-5 currents with an apparent pK of 7.2. The simplest explanation of this pH dependence would be that a larger concentration of protons directly increases the outward H^+ transport—because more protons are available. Recently, however, we have proposed a model for the transport activity of ClC-5 (Zdebik *et al*, 2008), in which transport does not take place continuously, but rather occurs in bursts, and pH could regulate the probability of the transporter to be in the active, transporting conformation. In the framework of this model, the mean current during a burst of activity, the 'single transporter current', directly reflects the elementary turnover rate. We found that the single transporter current is pH independent in the range between pH 5.3 and 7.3. This suggests that internal pH does not influence the turnover rate, but rather modulates the duration and/or the frequency of the bursts of transport. In other words, our results indicate that intracellular acidification exerts an effect by increasing the probability for ClC-5 to be in an active, transporting state. Furthermore, this result implies that for pH $\leqslant$7.3, H^+ delivery from the bulk intracellular solution to the transporter is not a rate-limiting step in the transport cycle. These measurements in external Cl^-, the physiologically relevant anion for ClC-5, were corroborated by analogous measurements in extracellular NO_3^-. As NO_3^- transport is associated with a greatly reduced H^+ transport, *a priori*, a drastically altered pH dependence might be expected. However, we found that NO_3^- transport has a very similar pH dependence as Cl^- transport, supporting our conclusion that pH_{int} does not directly impinge on the single transporter turnover rate. It is noteworthy that the single transporter current in NO_3^- is not larger than that in Cl^- (it is actually slightly smaller), indicating that the tighter coupling in Cl^- is not associated with a reduced capacity of ion transport. On the contrary, it appears that the slippage occurring in NO_3^- is associated with a less-efficient overall transport. We therefore interpret the increased macroscopic current seen in NO_3^- as an increased probability of the transporter to be in the active state in the presence of NO_3^-. Nevertheless, it should be kept in mind that noise analysis is an indirect method and that in the absence of

direct measurements of a single transporter turnover, these considerations have to be regarded with some caution.

The activation kinetics of ClC-5 currents upon voltage jumps to positive potentials are much more pronounced in NO_3^- than in Cl^-. This finding by itself provides additional support for the concept of a 'gated' transporter: the probability of the transporter to be in an active, transporting state is voltage dependent. This probability depends on the permeating anion, a feature well known from CLC Cl^- channels (Pusch *et al*, 1995).

Independently of the precise biophysical mechanism, our results suggest that modulation of ClC-5 by intracellular pH is physiologically relevant, for example to regulate the degree of endosomal acidification. In this regard, it is interesting to note that transcellular pH gradients have been described in proximal tubule cells (Aw and Jones, 1989), and that it has been reported that intracellular pH progressively declines along the proximal tubule (Pastoriza-Munoz *et al*, 1987).

Materials and methods

Molecular biology and oocyte expression

Human ClC-5 and ZmSut1 were expressed in *Xenopus* oocytes as described previously (Carpaneto *et al*, 2005; Picollo and Pusch, 2005). Oocytes were kept in a solution containing (in mM) 90 NaCl, 10 HEPES, 2 KCl, 1 $MgCl_2$, 1 $CaCl_2$, pH 7.5, for 3–6 days (ClC-5) or for 2–5 days (ZmSut1) at 18°C.

Patch clamp measurements and noise analysis

Inside-out patch clamp measurements were performed as described by Zdebik *et al* (2008). Briefly, patch pipettes were pulled from aluminosilicate capillaries (Hilgenberg, Malsfeld, Germany), coated with Sylgard, and fire-polished to a resistance of approximately 0.5–1 MΩ. The extracellular (pipette) solution contained (in mM) 100 NMDGCl, 10 HEPES, 5 $MgCl_2$, pH 7.3. The standard intracellular solution contained 100 mM NMDGCl, 10 HEPES, 2 $MgCl_2$, 1 EGTA, pH 7.3. The pH was adjusted with NaOH or H_2SO_4 to the desired values. For pH <7.3 MES buffer and for pH 9.3 Bis-Tris-propane buffer were used instead of HEPES. For patch measurements with external NO_3^-, the pipette solution contained (in mM) 100 NMDG-NO_3, 10 HEPES, 5 $MgCl_2$, pH 7.3. The 10 mM Cl^- arising from the $MgCl_2$ in this solution served to maintain a stable electrode potential. Control whole-oocyte two-electrode voltage-clamp and acidification measurements showed that this low concentration of Cl^- had a negligible influence on the current magnitude and H^+ transport activity. Solutions were changed by inserting the patch-pipette into the opening of ~0.5-mm-diameter glass perfusion capillaries. Perfusion flow was driven by gravity. Data for non-stationary noise analysis were obtained by repeatedly applying a voltage step to 140 mV. The mean current, I, and the variance, σ^2, were calculated from these traces as described (Zdebik *et al*, 2008), and the variance was plotted as a function of the mean current and fitted to the following equation

$$\sigma^2 = iI - \frac{I^2}{N} \quad (1)$$

where i is the apparent single transporter current and N the number of 'channels'.

Two-electrode voltage-clamp

Two-electrode voltage-clamp was performed with a Turbotec 03 amplifier (npi, Tamm, Germany) and a custom acquisition program (GePulse) at room temperature (20–25°C) as described earlier (Zdebik *et al*, 2008). The standard bath solution contained (in mM): 100 NaCl, 4 $MgSO_4$, 10 HEPES, pH 7.3. For measurements of the anion conductivity, NaCl was substituted with equimolar amounts of $NaNO_3$, NaBr, or NaI. For the analysis shown in Figure 4, the contribution of leak currents was estimated and subtracted assuming a linear leak conductance and assuming that currents at voltages more negative than −20 mV were pure leak.

Extracellular pH measurements using a pH-sensitive microelectrode

Proton transport was qualitatively measured by monitoring the acidification of the extracellular solution close to the oocyte using a pH-sensitive microelectrode as described previously (Picollo and Pusch, 2005; Zdebik *et al*, 2008). Briefly, a silanized microelectrode was tip-filled with a proton ionophore (Cocktail B, Fluka), back-filled with a solution containing a phosphate-buffered saline, and connected to a custom high-impedance amplifier. The electrodes were routinely checked and responded consistently with a slope of 57–61 mV/pH unit. The pH-sensitive microelectrode was pushed gently onto the vitelline membrane without rupturing the plasma membrane. The oocyte was simultaneously voltage-clamped and acidification was induced by applying a train of voltage-clamp pulses to a positive test potential. Solutions contained 0.5 mM buffer (HEPES for pH>6.5, otherwise MES).

Determination of the relative coupling efficiency

The microelectrode method cannot be used to determine absolute coupling coefficients. However, comparing measurements in the presence of different anions performed on the same oocyte with the pH-sensitive microelectrode in the same position, the relative coupling efficiency of anion/proton exchange was estimated in the following way. We applied a train of defined length of activating voltage pulses and measured the final change in extracellular pH, ΔpH, and the net current during the voltage pulses, I_{net}, in the presence of Cl^- or NO_3^- from the same oocyte. The current is the sum of the proton current, I_H, and the anion current, I_{anion}, and the latter is equal to $r_{anion} \cdot I_H$, where r_{anion} is the number of anions transported for each proton:

$$I_{net} = I_H + I_{anion} = (1 + r_{anion})I_H$$

As a first approximation, the acidification is proportional to the proton current:

$$\Delta pH \sim I_H$$

and thus

$$\frac{I_{net}}{\Delta pH} = f(1 + r_{anion}).$$

The proportionality factor, f, depends on the distance of the microelectrode from the oocyte surface, the local density of membrane expression, and other unknown factors. For the same oocyte and microelectrode position, however, f is identical for Cl^- and NO_3^-. Therefore, the ratio of these quantities in Cl^- and NO_3^-, respectively, defining the relative coupling efficiency, e_{rel},

$$e_{rel} = \frac{I_{net}(Cl)}{\Delta pH(Cl)} \frac{\Delta pH(NO_3)}{I_{net}(NO_3)} = \frac{1 + r_{Cl}}{1 + r_{NO_3}} \quad (2)$$

is a measure of the relative efficiency of NO_3^-/H^+ exchange compared with Cl^-/H^+ exchange. A small value of e_{rel} indicates that NO_3^- transport is less coupled than Cl^- transport, that is, $r_{NO_3} > r_{Cl}$.

Fluorescence-based measurements of proton transport

For ClC-5, the solution contained (in mM) 120 NaCl and 4 $MgCl_2$, 0.2 BCECF (Sigma, Milan), pH 7.3 (with NaOH). For ZmSut1, the control solution contained (in mM) 150 sorbitol, 30 NaCl, 4 $MgCl_2$, 0.2 MES, pH 6, whereas the measuring solution contained 120 sorbitol, 30 sucrose, 30 NaCl, 0.2 BCECF, pH 6. Thus, BCECF was the only buffer for the fluorescence measurements. Fluorescence was evoked and measured using a Till monochromator-based imaging system with an Imago cooled CCD camera mounted on an Axiovert Zeiss microscope and controlled by TillVision software (Till photonics, München, Germany). Fluorescence was excited alternately at 490 and 440 nm with 1 ms excitation duration, acquiring a pair of images every 100 ms using a 515 nm emission filter. The fluorescence ratio (490/440) was calculated online. A trigger from TillVision synchronously started a voltage-clamp pulse protocol to initiate proton flux and to record the transmembrane current. For ClC-5, the voltage protocol consisted of a 3- to 5-s-long depolarization to a voltage ranging from 20 to 120 mV. For ZmSut1, the voltage was first held at a positive value (from 20 to 40 mV) to minimize proton transport (Carpaneto *et al*, 2005) and was then switched to a test value (from −100 to −40 mV) to evoke H^+ influx. For ClC-5, leak currents were estimated from current responses to

negative voltages, and subtracted. For ZmSut1, leak currents were estimated from the current response in the absence of sucrose, and subtracted.

For calibration, 150 or 200 µl test solution were placed in the recording chamber, and fluorescence ratios were measured after successive addition of 2.5 µl of 1 mM NaOH (for ZmSut1 measurements) or 1 mM HCl (for ClC-5). The fluorescence ratio changed linearly with the amount of protons (or OH^-) added (see Figure 1B), and the slope of this relationship was used to convert fluorescence ratios into changes of total proton concentration. Calibration was performed before and after a set of experiments. BCECF solutions were prepared freshly before use.

The experimental fluorescence ratios were analysed as described in detail in the Supplementary data, to extract the net transmembrane proton current.

Supplementary data

Supplementary data are available at *The EMBO Journal* Online (http://www.embojournal.org).

Acknowledgements

We thank Drs Armando Carpaneto and Rainer Hedrich for the ZmSut1 clone, Thomas J Jentsch for the CLC clones, Anna Rosa Murgia for excellent technical assistance, Giacomo Gaggero for help in constructing the perfusion system and Enrico and Giacomo Gaggero for constructing the high-impedance amplifier. The financial support by Telethon, Italy (grants GGP04018 and GGP08064) is gratefully acknowledged.

References

Accardi A, Lobet S, Williams C, Miller C, Dutzler R (2006) Synergism between halide binding and proton transport in a CLC-type exchanger. *J Mol Biol* **362:** 691–699

Accardi A, Miller C (2004) Secondary active transport mediated by a prokaryotic homologue of ClC Cl^- channels. *Nature* **427:** 803–807

Aw TY, Jones DP (1989) Heterogeneity of pH in the aqueous cytoplasm of renal proximal tubule cells. *FASEB J* **3:** 52–58

Carpaneto A, Geiger D, Bamberg E, Sauer N, Fromm J, Hedrich R (2005) Phloem-localized, proton-coupled sucrose carrier ZmSUT1 mediates sucrose efflux under the control of the sucrose gradient and the proton motive force. *J Biol Chem* **280:** 21437–21443

De Angeli A, Monachello D, Ephritikhine G, Frachisse JM, Thomine S, Gambale F, Barbier-Brygoo H (2006) The nitrate/proton antiporter AtCLCa mediates nitrate accumulation in plant vacuoles. *Nature* **442:** 939–942

Dutzler R, Campbell EB, Cadene M, Chait BT, MacKinnon R (2002) X-ray structure of a ClC chloride channel at 3.0 Å reveals the molecular basis of anion selectivity. *Nature* **415:** 287–294

Dutzler R, Campbell EB, MacKinnon R (2003) Gating the selectivity filter in ClC chloride channels. *Science* **300:** 108–112

Friedrich T, Breiderhoff T, Jentsch TJ (1999) Mutational analysis demonstrates that ClC-4 and ClC-5 directly mediate plasma membrane currents. *J Biol Chem* **274:** 896–902

Gadsby DC (2004) Ion transport: spot the difference. *Nature* **427:** 795–797

Graves AR, Curran PK, Smith CL, Mindell JA (2008) The Cl^-/H^+ antiporter ClC-7 is the primary chloride permeation pathway in lysosomes. *Nature* **453:** 788–792

Günther W, Lüchow A, Cluzeaud F, Vandewalle A, Jentsch TJ (1998) ClC-5, the chloride channel mutated in Dent's disease, colocalizes with the proton pump in endocytotically active kidney cells. *Proc Natl Acad Sci USA* **95:** 8075–8080

Günther W, Piwon N, Jentsch TJ (2003) The ClC-5 chloride channel knock-out mouse—an animal model for Dent's disease. *Pflügers Arch* **445:** 456–462

Hara-Chikuma M, Wang Y, Guggino SE, Guggino WB, Verkman AS (2005) Impaired acidification in early endosomes of ClC-5 deficient proximal tubule. *Biochem Biophys Res Commun* **329:** 941–946

Hilgemann DW (1996) Unitary cardiac Na^+, Ca^{2+} exchange current magnitudes determined from channel-like noise and charge movements of ion transport. *Biophys J* **71:** 759–768

Jayaram H, Accardi A, Wu F, Williams C, Miller C (2008) Ion permeation through a Cl^--selective channel designed from a CLC Cl^-/H^+ exchanger. *Proc Natl Acad Sci USA* **105:** 11194–11199

Jentsch TJ (2005) Chloride transport in the kidney: lessons from human disease and knockout mice. *J Am Soc Nephrol* **16:** 1549–1561

Jentsch TJ (2008) CLC chloride channels and transporters: from genes to protein structure, pathology and physiology. *Crit Rev Biochem Mol Biol* **43:** 3–36

Lloyd SE, Pearce SH, Fisher SE, Steinmeyer K, Schwappach B, Scheinman SJ, Harding B, Bolino A, Devoto M, Goodyer P, Rigden SP, Wrong O, Jentsch TJ, Craig IW, Thakker RV (1996) A common molecular basis for three inherited kidney stone diseases. *Nature* **379:** 445–449

Lobet S, Dutzler R (2006) Ion-binding properties of the ClC chloride selectivity filter. *EMBO J* **25:** 24–33

Ludewig U, Pusch M, Jentsch TJ (1996) Two physically distinct pores in the dimeric ClC-0 chloride channel. *Nature* **383:** 340–343

Maduke M, Miller C, Mindell JA (2000) A decade of CLC chloride channels: structure, mechanism, and many unsettled questions. *Annu Rev Biophys Biomol Struct* **29:** 411–438

Middleton RE, Pheasant DJ, Miller C (1996) Homodimeric architecture of a ClC-type chloride ion channel. *Nature* **383:** 337–340

Miller C (2006) ClC chloride channels viewed through a transporter lens. *Nature* **440:** 484–489

Nguitragool W, Miller C (2006) Uncoupling of a CLC Cl(−)/H(+) exchange transporter by polyatomic anions. *J Mol Biol* **362:** 682–690

Pastoriza-Munoz E, Harrington RM, Graber ML (1987) Axial heterogeneity of intracellular pH in rat proximal convoluted tubule. *J Clin Invest* **80:** 207–215

Picollo A, Pusch M (2005) Chloride/proton antiporter activity of mammalian CLC proteins ClC-4 and ClC-5. *Nature* **436:** 420–423

Piwon N, Günther W, Schwake M, Bösl MR, Jentsch TJ (2000) ClC-5 Cl^--channel disruption impairs endocytosis in a mouse model for Dent's disease. *Nature* **408:** 369–373

Pusch M, Ludewig U, Rehfeldt A, Jentsch TJ (1995) Gating of the voltage-dependent chloride channel CIC-0 by the permeant anion. *Nature* **373:** 527–531

Roos A, Boron WF (1981) Intracellular pH. *Physiol Rev* **61:** 296–434

Scheel O, Zdebik AA, Lourdel S, Jentsch TJ (2005) Voltage-dependent electrogenic chloride/proton exchange by endosomal CLC proteins. *Nature* **436:** 424–427

Steinmeyer K, Schwappach B, Bens M, Vandewalle A, Jentsch TJ (1995) Cloning and functional expression of rat CLC-5, a chloride channel related to kidney disease. *J Biol Chem* **270:** 31172–31177

Swietach P, Leem CH, Spitzer KW, Vaughan-Jones RD (2005) Experimental generation and computational modeling of intracellular pH gradients in cardiac myocytes. *Biophys J* **88:** 3018–3037

Walden M, Accardi A, Wu F, Xu C, Williams C, Miller C (2007) Uncoupling and turnover in a Cl^-/H^+ exchange transporter. *J Gen Physiol* **129:** 317–329

Weinreich F, Jentsch TJ (2001) Pores formed by single subunits in mixed dimers of different CLC chloride channels. *J Biol Chem* **276:** 2347–2353

Zdebik AA, Zifarelli G, Bergsdorf EY, Soliani P, Scheel O, Jentsch TJ, Pusch M (2008) Determinants of anion–proton coupling in mammalian endosomal CLC proteins. *J Biol Chem* **283:** 4219–4227

Zifarelli G, Pusch M (2007) CLC chloride channels and transporters: a biophysical and physiological perspective. *Rev Physiol Biochem Pharmacol* **158:** 23–76

Zifarelli G, Soliani P, Pusch M (2008) Buffered diffusion around a spherical proton pumping cell: a theoretical analysis. *Biophys J* **94:** 53–62

